Tau protein aggregation associated with SARS-CoV-2 main protease

Raphael Josef Eberle[1,2*], Mônika Aparecida Coronado[1], Ian Gering[1], Karolina Korostov[1], Anja Stefanski[3], Kai Stühler[3], Victoria Kraemer-Schulien[3], Lara Blömeke[1,2], Oliver Bannach[1,2,4], Dieter Willbold[1,2,5]

[1]Institute of Biological Information Processing (IBI-7: Structural Biochemistry), Forschungszentrum Jülich, Jülich, Germany.

[2]Institute of Physical Biology, Heinrich-Heine-University Düsseldorf, Düsseldorf, Germany.

[3]Molecular Proteomics Laboratory (MPL), BMFZ, Heinrich-Heine-University Düsseldorf, Düsseldorf, Germany.

[4]attyloid GmbH, 40225, Düsseldorf, Germany.

[5]JuStruct: Jülich Centre for Structural Biology, Forschungszentrum Jülich, Jülich, Germany.

*** Correspondence:**
r.eberle@fz-juelich.de

Abstract

The primary function of virus proteases is the proteolytic processing of the viral polyprotein. These enzymes can also cleave host cell proteins, which is important for viral pathogenicity, modulation of cellular processes, viral replication, the defeat of antiviral responses and modulation of the immune response. It is known that COVID-19 can influence multiple tissues or organs and that infection can damage the functionality of the brain in multiple ways. After COVID-19 infections, amyloid-β, neurogranin, tau and phosphorylated tau were detected extracellularly, implicating possible neurodegenerative processes.

The present study describes the possible induction of protein aggregation by the SARS-CoV-2 3CL protease ($3CL^{pro}$) possibly relevant in neuropathology, such as aggregation of tau, alpha-synuclein and TPD-43. Further investigations demonstrated that tau was proteolytically cleaved by the viral protease 3CL and, consequently, generated aggregates. However, more evidence is needed to confirm that COVID-19 is able to trigger neurodegenerative diseases.

Keywords: Tau, $3CL^{pro}$, SARS-CoV-2, Covid-19, aggregation, viral infection

Introduction

Viral pathogens encode their protease(s) or use host proteases for their replication cycle. In the case of acute respiratory syndrome coronavirus 2 (SARS-CoV-2), proteolytic cleavage of the two virus polyproteins generates the various viral proteins needed to form a replication complex required for transcription and replication of the viral genome and subgenomic mRNAs. The key viral enzymes responsible are the papain-like (PLP, nsp3) and 3-chymotrypsin-like proteases ($3CL^{pro}$) [1-3]. In addition, host cell protein cleavage is a critical component of viral pathogenicity [4], including diverting cellular processes to viral replication, defeating antiviral responses and immune response modulation. Many large-scale analyses of the SARS-CoV-2 infected-cell transcriptome, proteome, phosphoproteome and interactomes are described [5-7]. Regarding the $3CL^{pro}$ human substrate repertoire, also known as the degradome [8], Pablos et al., 2021 identified over 100 substrates and 58 additional high confidence candidate substrates out of SARS-CoV-2 infected human lung and kidney cells [9].

SARS-CoV-2 was identified in December 2019 as the causative agent of coronavirus disease-19 (COVID-19) first occurring in Wuhan, Hubei province, China [10]. According to the data that were reported to the World Health Organization (WHO) up to the 3rd of January 2023, the global SARS-CoV-2 pandemic was associated with >655 million confirmed cases of infections and >6.6 million virus-related deaths worldwide [11].

It is well known that SARS-CoV-2 infection can influence multiple tissues or organs [12-16]. Post-COVID syndrome (also known as Long-COVID) has also been described as a syndrome that encompasses a prolonged course of various physical and neuropsychiatric symptoms that persist for more than 12 weeks [17,18]. It has also been reported that COVID-19 can damage the brain in different ways (Table 1).

Table1. Some neurological symptoms caused by COVID-19.

Neurological symptom	Reference
Loss of smell (anosmia) and altered taste (ageusia)	[19]
Myoclonus, cerebellar ataxia, seizure and tremor	[20,21]
Headache	[22]
Cardiorespiratory failure	[23]
Encephalopathy	[24]
Acute Disseminated Encephalomyelitis	[25]
Stroke	[26]
Guillain-Barre syndrome	[27]

Douaud et al. 2022 described the dramatic effects of SARS-CoV-2 infections on the brain structure, including a reduction in grey matter thickness, tissue damage in regions that are functionally connected

to the primary olfactory cortex and a significant reduction in global brain size [28]. However, so far, there exists no direct link with the generation of neurodegenerative diseases like Parkinson's disease (PD), Alzheimer's disease (AD), amyotrophic lateral sclerosis (ALS), frontotemporal dementia (FTD), Huntington's disease (HD), spinocerebellar ataxias, corticobasal degeneration, progressive supranuclear palsy, chronic traumatic encephalopathy, or multiple system atrophy. These diseases have many common features, including their chronic and progressive nature, the increased prevalence with age, destruction of neurons in specific areas of the brain, damage to the network of synaptic connections, and selective brain mass loss [29]. Another event is the progressive accumulation of misfolded protein aggregates with well-ordered structures. The proteins most commonly implicated in the accumulation of cerebral misfolded aggregates include amyloid-beta (Aβ), tau, alpha-synuclein (α-Syn) and TAR DNA-binding protein 43 (TDP-43) [29].

After COVID-19 infections in the brain, amyloid-β, neurogranin, tau and phosphorylated tau can be detected extracellularly, implicating possible neurodegenerative processes [30]. Another study demonstrated that the spike protein receptor binding domain binds to heparin and heparin-binding proteins, including amyloid-β, α-synuclein, tau, prion and TDP-43, which may initiate the pathological aggregation of these proteins resulting in neurodegeneration [31,32]. Ramani et al. 2020 showed that SARS-CoV-2 targets neurons of 3D human brain organoids and neurons invaded with SARS-CoV-2 at the cortical area display altered tau, tau hyperphosphorylation distribution and apparent neuronal death [33].

Tau phosphorylation and tau proteolysis are likely key factors in disease-associated tau aggregation and accumulation. Tau proteolysis can destabilise its primary structure, preventing correct folding and can lead to the formation of aggregated tau species due to a disordered quaternary structure. Tau can be cleaved by various proteolytic enzymes, including caspases, calpains, thrombin, cathepsins, metalloprotease 10, asparagine endopeptidase and puromycin-sensitive aminopeptidase [34].

Here, we report the cleavage and aggregation of tau after SARS-CoV-2 $3CL^{pro}$ treatment *in vitro* using a combination of ThT assays, analytical HPLC and mass spectrometry.

Material and Methods

Preparation of alpha-synuclein, TDP-43 and 2N4R tau

Alpha-synuclein was cloned, expressed and purified, as described previously [35]. TDP-43 sample was kindly provided by Dr Jeanine Kutzsche (IBI-7, Forschungszentrum Jülich). The gene for human tau (2N4R) encodes a protein of 441 amino acids. The respective gene was commercially synthesised

and cloned into the pET28A(+) vector (Genentech, San Francisco, USA), without His-tag. Protein expression was performed as described previously [36].

Protein extraction began by dissolving the cell pellet of 1 L expression in 30 ml buffer 1 (50 mM HEPES pH 7.5, 500 mM KCL, 5 mM β-ME and 1 mM EDTA). The dissolved cell pellets were heated for 30 min at 85 °C followed by 10 min on ice, and samples were sonicated 3 x 40 seconds at a power setting of 5 in an ultrasonic cell disruptor Modell 250 (Branson Ultrasonic, Brookfield, USA). Bacterial debris was pelleted for 50 min at 10,000 x g. Soluble tau protein was precipitated from the supernatant by adding 40 ml of a saturated ammonium sulfate solution and incubated for 30 minutes at room temperature. Afterwards, the samples were centrifuged for 30 min at 10,000 x g, and the pellet was resuspended in buffer 2 (50 mM HEPES pH 7.5, 50 mM KCL, 1.5 M ammonium sulfate, 2 mM TCEP and 1 mM EDTA). The solution was centrifuged for 30 minutes at 10,000 x g, and the pellet was resolved in 10 mL ddH_2O and 2 mM TCEP. The sample was centrifuged again for 30 minutes at 10,000 x g, and the appearing pellet was resuspended in buffer 3 (20 mM HEPES pH 6.7, 150 mM NaCl, 2 mM TCEP and 1 mM EDTA). The sample was centrifuged for 1h at 12,000 x g, and the supernatant was dialysed overnight at 6 °C against buffer 4 (50 mM ammonium acetate pH 7.4, 1 mM TCEP). The protein purity was assessed by SDS/PAGE (15%).

Western Blot with fluorescent tau13 antibody

For western blots, a fluorescent anti-tau antibody was used. Therefore tau13 (Biolegend, San Diego, USA) was labelled with CF633 (Biotium, Freemont, USA), and the labelling process was performed as described previously [37]. 2N4R tau recombinant protein samples were prepared in Laemmli buffer (final 1× composition: 20 mM Tris, pH 6.8, 2% SDS, 6% glycerol, 1% β-ME, 0.002% Bromophenol Blue). All samples were heated at 95 °C for 5 min and separated using SDS PAGE (15%). Proteins were then transferred to a polyvinylidene fluoride (PVDF) membrane (Thermo Fisher Scientific, Waltham, USA) at 500 mA for 40 min. After a washing step for 15 min in Tris-buffered saline tween buffer (TBS-T) (20 mM Tris, 150 mM NaCl, 0.1% Tween 20), the membrane was blocked for 1 h with 2.5% milk powder/TBS-T. Next, the membrane was washed with TBS-T, 2 × 5 min and in the last step for 15 min. Tau13 stocks were 1 mg/ml and were diluted in TBS-T (1:5000). The membrane was incubated with the antibody for 1.5 h. at RT. After a final wash step (2 × 5 min and 1 × 10 min), TBS-T was performed. Detection based on the CF633 fluorescence of the labelled tau13 antibody. Bio-Rad universal hood II and Chemidoc XRS camera and Quantity One 4.6.5 software enabled the visualisation and quantification of the protein bands.

Cloning, expression and purification of SARS-CoV-2 3CL^{pro}

SARS-CoV-2 3CL^{pro} (Uniprot entry: P0DTD1, virus strain: hCoV-19/Wuhan/WIV04/2019) was cloned, expressed and purified, as described previously [38].

Thioflavin T Aggregation (ThT) Assay

ThT aggregation assays were conducted in Corning half area 96-well plates with the non-binding surface (Corning No. 3881, Glendale, AZ, USA). As a control, polymerisation of 2N4R tau was initiated in the presence of the aggregation inducer heparin (Sigma-Aldrich, USA) with a molar ratio of 4:1 (Tau:heparin). 10 µM tau was incubated with 2.5 µM heparin (the final volume of the reaction mixture was 150 µl). The experiment buffer contained 20 mM Tris pH 7.2, 200 mM NaCl, 1 mM TCEP and 10 µM ThT. Fluorescence intensities were measured at 6 minutes intervals over 30 hours at 350 rpm and 37˚C using an Infinite 200 PRO plate reader (Tecan, Männedorf, Switzerland). The excitation and emission wavelengths were 440 and 490 nm, respectively. All measurements were performed in triplicate, and data are presented as mean ± SD.

Thioflavin T Aggregation (ThT) Assay using SARS-CoV-2 3CL^{pro} as the inducer

ThT assays were performed as described before. Instead of heparin, 10 µM SARS-CoV-2 3CL^{pro} was used as an aggregation inducer. In a preliminary test, the effect of 3CL^{pro} against 10 µM 2N4R tau, α synuclein and TDP-43 was tested over 24h. As a control, the same experiment was performed with the single proteins.

A further experiment was performed with inactivated 3CL^{pro}, the protease was incubated with an equimolar concentration of Disulfiram (DSF) (10µM) for 30 minutes at RT, after 10 µM 2N4R tau and ThT was added, and the experiment was running for 24h. As a control, 2N4R tau was incubated with DSF and monitored for the same experimental time.

Furthermore, a ThT assay of 10 µM tau and 3CL^{pro} were stopped after 24h, and the protease was inactivated through DSF addition (10 µM) and incubated for 30 minutes at RT. Afterwards, a new tau sample (10µM) was added. The same procedure without inactivating the protease was followed as a control. All measurements were performed in triplicate, and data are presented as mean ± SD.

Investigation of tau and 3CL^{pro} doses dependency

Different concentrations were titrated to investigate tau, and 3CLpro doses dependency on the 2N4R tau fibril formation and a ThT assay was performed as described before. The effect of 0, 2.5, 5,

10, 25 and 50 µM $3CL^{pro}$ was tested against 10 µM tau over 24h. We also tested the opposite effect, where 0, 5, 10, 20, 40, 60, 80, and 100 µM of tau were tested against 10 µM $3CL^{pro}$. All experiments were performed in triplicate, and data are presented as mean ± SD.

Stability of tau in the presence of Sars-CoV-2 $3CL^{pro}$ investigated by High-performance liquid chromatography

To explore the proteolytic degradation of tau by $3CL^{pro}$ samples after 0, 24, 48 and 72 h incubation were analysed by high-performance liquid chromatography (HPLC). Agilent 1260 Infinity II system (Agilent Technologies, Santa Clara, CA, USA), equipped with a quaternary pump, autosampler, heated column compartment, multi-wavelength detector (MWD) and an analytical fraction collector, was used. 20 µL of sample solution was injected into an Agilent Zorbax 300-SB C8 4.6*250 mm, 5 µm reversed-phase liquid chromatography column (Agilent Technologies, Santa Clara, CA, USA), which was heated to 80 °C. Mobile phases consisted of A: Water + 0.1% Trifluoroacetic acid (TFA) and B: Acetonitrile + 0.1% TFA. Analyte elution was accomplished by a linear gradient from 10% to 80% buffer B in 20 min. Chromatograms were acquired at 214 nm and 280 nm. Furthermore, data acquisition and evaluation were performed with the Agilent OpenLab software (Version 2.6). The mean peak area of each triplicate was plotted against incubation time. Chromatograms of tau with $3CL^{pro}$ and chromatograms with a single protein were investigated for metabolite formation after an incubation period of up to 72 h. The peaks related to the sample in which both proteins were present (max incubation 72 h) were considered potential metabolites of the tau protein produced by Sars-CoV-2 $3CL^{pro}$.

Purification of tau metabolites after proteolytic degradation by Sars-CoV-2 $3CL^{pro}$

To further investigate tau metabolites produced by incubation with Sars-CoV-2 $3CL^{pro}$, we used HPLC and further mass spectrometry (MS) analysis. Tau was incubated with the protease for 72h at 37 °C and 500 rpm. HPLC conditions were the same as described above. 100 µL of the sample was applied to the column per each chromatography run, and fractions were collected every minute. Fractions containing the same peak were pooled and lyophilised; subsequently, the samples were submitted for MS analysis.

Sample processing and mass spectrometry

Lyophilised samples were resuspended in 500 µL 0.1% trifluoroacetic acid (TFA) and digested with trypsin (Serva, Heidelberg, Germany) in 50 mM NH_4HCO_3 overnight at 37 °C. Tryptic peptides were extracted with 0.1% TFA and subjected to MS-coupled liquid chromatography. Briefly, for peptide separation over a 55-minute LC-gradient with 300 nL/min in an Ultimate 3000 Rapid Separation liquid chromatography system (Thermo Scientific, Bremen, Germany) equipped with an Acclaim PepMap 100 C18 column (75 µm inner diameter, 25 cm length, 2 mm particle size from Thermo Scientific, Bremen, Germany) was used. MS analysis was carried out on a Q-Exactive plus mass spectrometer (Thermo Scientific, Bremen, Germany) operating in positive mode and equipped with a nanoelectrospray ionisation source. The capillary temperature was set to 250 °C and the source voltage to 1.5 kV. Survey scans were carried out over a mass range from 200-2,000 m/z at a resolution of 70,000 (at 200 m/z). The target value for the automatic gain control was 3,000,000, and the maximum fills time was 50 ms. The 20 most intense peptide ions (excluding singly charged ions) were selected for fragmentation. Peptide fragments were analysed using a maximal fill time of 50 ms, automatic gain control target value of 100,000 and a resolution of 17,500 (at 200 m/z). Already fragmented ions were excluded for fragmentation for 10 seconds.

Acquired spectra were searched using Sequest HT within Proteome Discoverer version 2.4.1.15 against the SwissProt *Homo sapiens* proteome dataset (UP000005640, 75777 sequences) with the inserted sequence of the human tau protein and an *E.coli* BL21 (DE3) database (UP000002032, 4156 sequences). Methionine oxidation was considered a variable modification and tryptic cleavage specificity with a maximum of two missed cleavage sites. For the main search, a precursor mass tolerance of 10 ppm and a mass tolerance of 0.02 Da were applied for fragment spectra. For the semi-specific tryptic search of peptides, PEAKS Studio 10.6 Build 220201221 was used, and the above human database was searched with an error tolerance of 20 ppm for parent masses and an error tolerance of 0.2 Da for fragment masses.

Surface-based fluorescence intensity distribution analysis

To quantify tau aggregation due to $3CL^{pro}$ activity, surface-based fluorescence intensity distribution analysis (sFIDA) was performed according to the biochemical principle of Kravchenko et al. 2017, and Herrmann et al. 2017 [39,40]. Therefore, we used 384-Well plates (Greiner, Kremsmünster, Austria) to incubate the capture-antibody tau12 in 0.1 M carbonate at a 2.5 µg/ml concentration. After a fivefold washing step with TBS-T and TBS, 80 µl of blocking solution (Candor Bioscience, Wangen, Germany)

was added and incubated for 1.5 h. Afterwards, the plate was washed like previously described, and 20 µl of tau conjugated silica-nanoparticles (SiNaPs) and tau aggregates diluted in low cross buffer strong (Candor Bioscience GmbH, Wangen in Allgäu, Germany) were added. In Addition, 20 µl of 10 nM and 100 nM tau monomer were applied.

To investigate the formation of tau oligomers or aggregates induced by $3CL^{pro}$, 5 µM tau monomer was incubated with 5 µM $3CL^{pro}$ for 72 h. The negative control was established equivalently; however, the protease was previously inactivated with 10 µM Disulfiram (DSF).

The samples, buffer control (BC) and capture control (CC), were incubated for 2 h and washed five times with TBS. For capture control, the capture antibody was omitted. As a detection probe, 20 µl of 0.078 µg/ml tau13 CF633 in TBS was used. After 1 h of incubation, the wells were washed five times with TBS, and the buffer was changed against TBS-ProClin. The SiNaPs and antibodies used were synthesised and labelled according to the previously described principle [37,41].

Results and Discussion

Purification of 2N4R tau with a precipitation approach and characterisation of the protein

2N4R tau was expressed in BL21 (DE3) (T1) *E. coli* and purified by a precipitation approach. 2N4R tau consists of 266 amino acids with an approximated molecular weight of 46 kDa. The purity was assessed by SDS PAGE (Supplementary figure S1). However, the protein presented a single band on a denaturing SDS-PAGE gel with an apparent molecular mass of 60 kDa. A western blot with the specific antibody (Tau13, Biolegend) confirmed the target protein (Supplementary figure S2A). Following successful purification, 2N4R tau was characterised to compare the properties to those previously reported [42-45]. It is well known that tau, in the monomeric state, is inherently unfolded, with predominantly random-coil conformation. Our CD analysis confirmed this observation for the purified protein, with minimum peaks around 200 nm (Supplementary figure S2B). Tau aggregation was investigated using ThT assay and heparin as an inducer [46]. The results of the ThT assay indicated that heparin promoted the induction and acceleration of tau aggregation within 24h (Supplementary figure S2C). The structural changes of tau in the presence of heparin were followed by CD spectroscopy, demonstrating a shift of the absorbance spectrum from 202 (random-coil conformation) to 213 (beta-sheet conformation) nm (Supplementary figure S2B). Those results demonstrated that tau had been successfully aggregated by heparin because the aggregation of this protein is characterised by a transition from random coil to beta-sheet conformation [43].

Identification and characterisation of tau aggregation events induced by SARS-CoV-2 3CL^{pro} using ThT assay

To identify a possible aggregation effect caused by SARS-CoV-2 3CL^{pro} on tau, alpha-synuclein and TDP-43 proteins, a ThT fibrillation assay was performed. The preliminary test showed that tau aggregates increased over time after the addition of 10 µM of SARS-CoV-2 3CL^{pro}, which was not observed for alpha-synuclein and TDP-43 (Fig. 1A). To confirm our preliminary results, control experiments using the single proteins was performed, which indicated no signal of aggregation over the time (Fig. 1B).

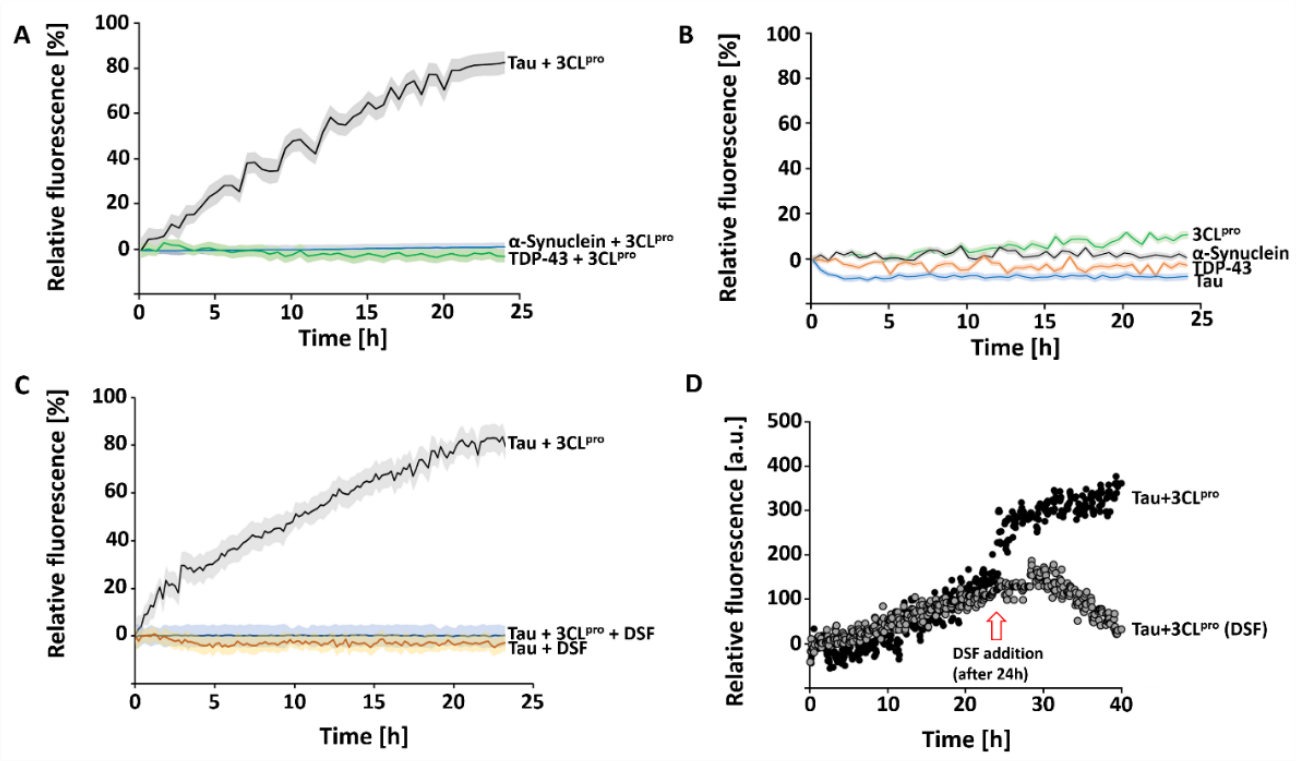

Figure 1. Effect of SARS-CoV-2 3CL^{pro} on 2N4R tau aggregation and effect of 3CL^{pro} inactivation on tau aggregation A: ThT assay of 2N4R tau, α-Synuclein and TDP-43, 3CL^{pro} used as aggregation inducer. The experiment was performed for 24 h, 37 °C and 600 rpm. **B:** Control ThT assay of single 3CL^{pro}, α-Synuclein, TDP-43 and tau. The inactivation of the protease was treated with 10 µM DSF. **C:** ThT assay of inactivated 3CL^{pro}, tau aggregation was not observed. **D:** ThT assay of 2N4R tau, aggregation was induced by 3CL^{pro}. After 24h DSF inactivated the protease and after 30 minutes of incubation, 10 µM fresh tau was added. Data shown are the mean ± SD from three independent measurements (n=3).

Additional ThT experiments were performed to evaluate the dose dependency of SARS-CoV-2 3CL^{pro} and 2N4R tau concentration on the aggregation behaviour of tau. A higher concentration of the protease (0, 0.5, 1, 2.5, 5 and 10 µM) caused a higher amount of the tau aggregates in a given time of 24h (Supplementary fig. S3A). Similarly, the titration of tau at different concentrations (0, 5, 10, 20, 40, 60, 80 and 100 µM) demonstrated that the monomer concentration and its cleavage are accompanied by the amount of aggregate formation (Supplementary fig. S3B).

Effect of SARS-CoV-2 3CL^{pro} inactivation on tau aggregation

There exist two possibilities for how SARS-CoV-2 3CL^{pro} induced tau aggregation: (1) both proteins interact and form aggregates; (2) the protease cleaves tau and thus produces insoluble fragments that will initiate the aggregation process. To discover the possible forms of the aggregation endured by tau protein, we performed ThT assays using inactivated 3CL^{pro} by disulfiram (DSF), a known 3CL^{pro} inhibitor [47]. The results demonstrated that inactivation of the protease prevents tau aggregation (Fig. 1C), which allows us to suggest that the proteolysis role of the 3CLpro initiates the aggregation process. The addition of DSF in a running ThT assay stopped the tau aggregation immediately (Fig. 1D).

Stability of tau under SARS-CoV-2 3CL^{pro} influence

The stability of 2N4R tau under the influence of SARS-CoV-2 3CL^{pro} was investigated using analytical HPLC experiments. Interestingly, the results demonstrated an evident cleavage of tau protein by the virus protease (Fig. 2). As described before, the protein mix was analysed over 0, 24, 48 and 72 h of incubation. The corresponding tau monomer peak (I) (retention time: 10.6 minutes) in the chromatogram decreased over 72h (Fig. 2A), which can also be observed in a silver-stained SDS PAGE (Fig. 2C). Beside the reduction of the monomer form of tau the presence of a new protein band around 25 kDa was observed, which allow us to suggest that it represents the tau fragments after the 3CL^{pro} proteolytic effect. Additionally, two additional peaks were observed on the analytical HPLC chromatogram (II, III) (Fig. 2A, D and E). SDS PAGE analysis of the related fractions (regions II and III) also validated the increasing protein bands over experimental time.

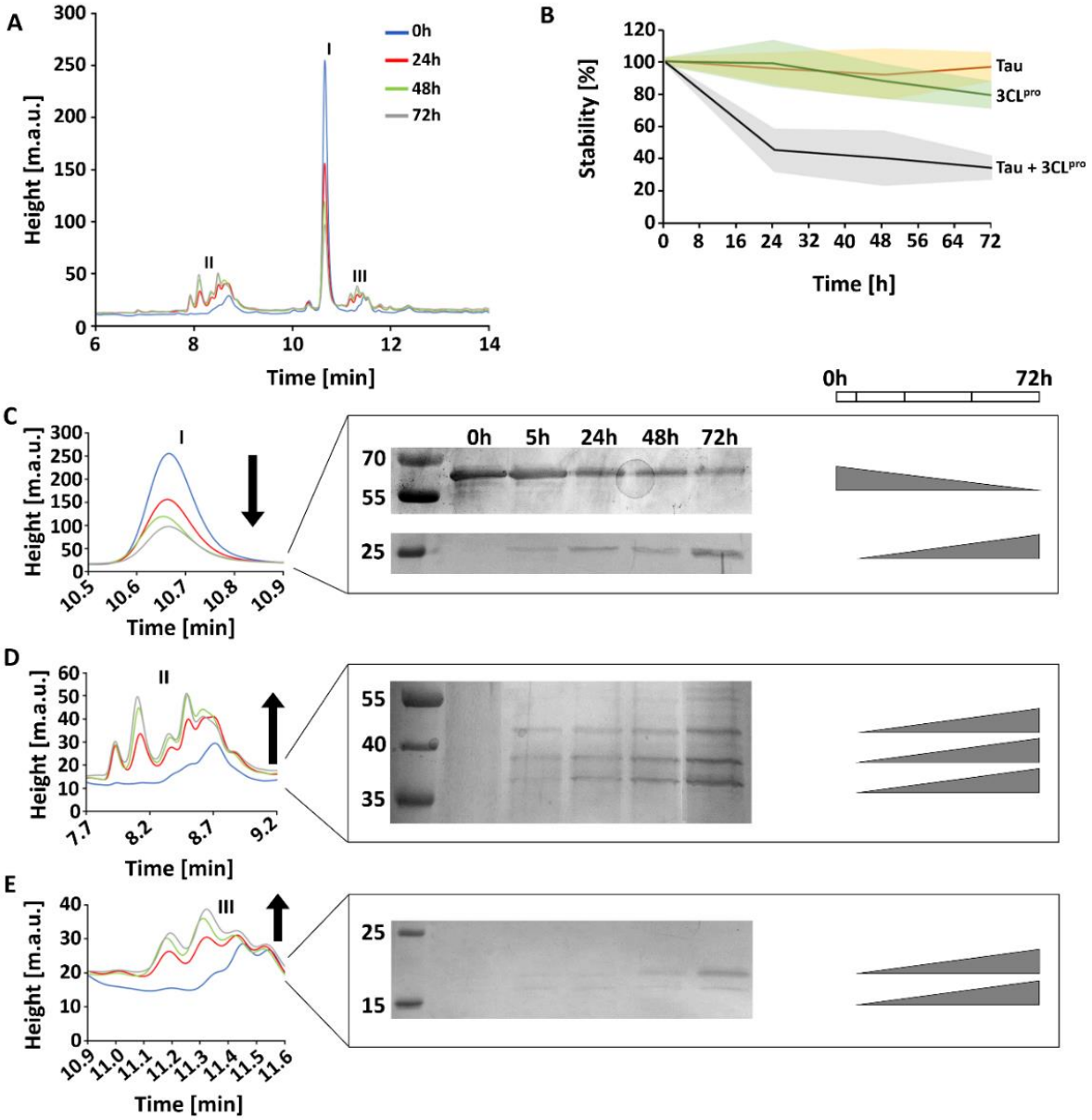

Figure 2. Effect of SARS-CoV-2 3CL^{pro} on 2N4R tau degradation. A: Analytical HPLC analysis of 2N4R tau incubated with SARS-CoV-2 3CL^{pro} for 0, 24, 48 and 72h. The corresponding chromatogram regions of the tau monomer and related metabolites are labelled (I-III). **B:** Stability of 2N4R tau monomer after treatment with 3CL^{pro} over 72h. Single tau and 3CL^{pro} are shown as control. After 3CL^{pro} treatment, the tau monomer amount decreases by about 60%. **C:** Chromatogram of peak I (Tau) shown enlarged, a silver stained SDS PAGE demonstrated that the 2N4R tau amount decreased over 72h treatment with 3CL^{pro} and a protein band increases at 25 kDa. **D:** Chromatogram of peak region II shows enlarged three protein bands appearing over 72h experimental time. **E:** Chromatogram of peak region III shown enlarged, two protein bands appear over the 72h experimental time.

Based on our results, we assumed that SARS-CoV-2 3CL^{pro} cleaves tau possibly in different sites, resulting in truncated tau species. After 72 h experimental time, the 2N4R tau amount was reduced by about 60% related to the start point. Interestingly, in the first 24 h, the degradation process declines substantially to about 50% of the monomer amount; however, during the remaining 48 h, the monomer amount reduced by just around 10% (Fig. 2B). This observation can be attributed to the diminished amount of the monomer itself.

HPLC experiments with 2N4R tau and inactivated $3CL^{pro}$ showed that the corresponding tau peak and the peak regions I, II and III are unaffected. After 72 h, tau is slightly depredated (~5%) (Supplementary Fig. S4).

Analysis of the tau digestion underwent $3CL^{pro}$ using mass spectrometry

We have used mass spectrometry (MS) experiments to confirm tau fragments in the HPLC peaks I, II and III. Untreated 2N4R tau was used as control; in all tested samples, tau could be detected (Fig. 3). The determination of tryptic tau peptides AEPRQEFEVMEDHAGTYGGLGDR, GDTPSLEDEAAGHVTQAR and SPQLATLADEVSASLAK are shown in Fig. 3A and supplementary figures S5 and S6. All tryptic tau peptides that were identified are listed in supplementary tables S1-S4 (Tryptic peptides that occurred less than three times are not shown).

In the tau control, 111 tryptic peptides could be determined, and AEPRQEFEVMEDHAGTYGGLGDR had the highest appearance (eight times). Interestingly, we could not identify, in fractions II and III, the N-terminal tryptic peptides detected in the control and peak I (AEPRQEFEVMEDHAGTYGGLGDR and AGLKESPLQTPTEDGSEEPGSETSDAKSTPTAEDVTAPLVDEGAPGKQ) (Fig. 3B). Additionally, tryptic peptides in the mid-region and C-terminus of the control sequence could not be detected in fractions related to peak I, II and III (TPPSSGEPPKSGDRSGYSSPGSPGTPGSR, QTAPVPMPDLK and TDHGAEIVYKSPVVSGD). Likewise, the peptide (GSLGNIHHKPGGGQVEVK) in control was not detected in the peak I sample (Fig. 3B).

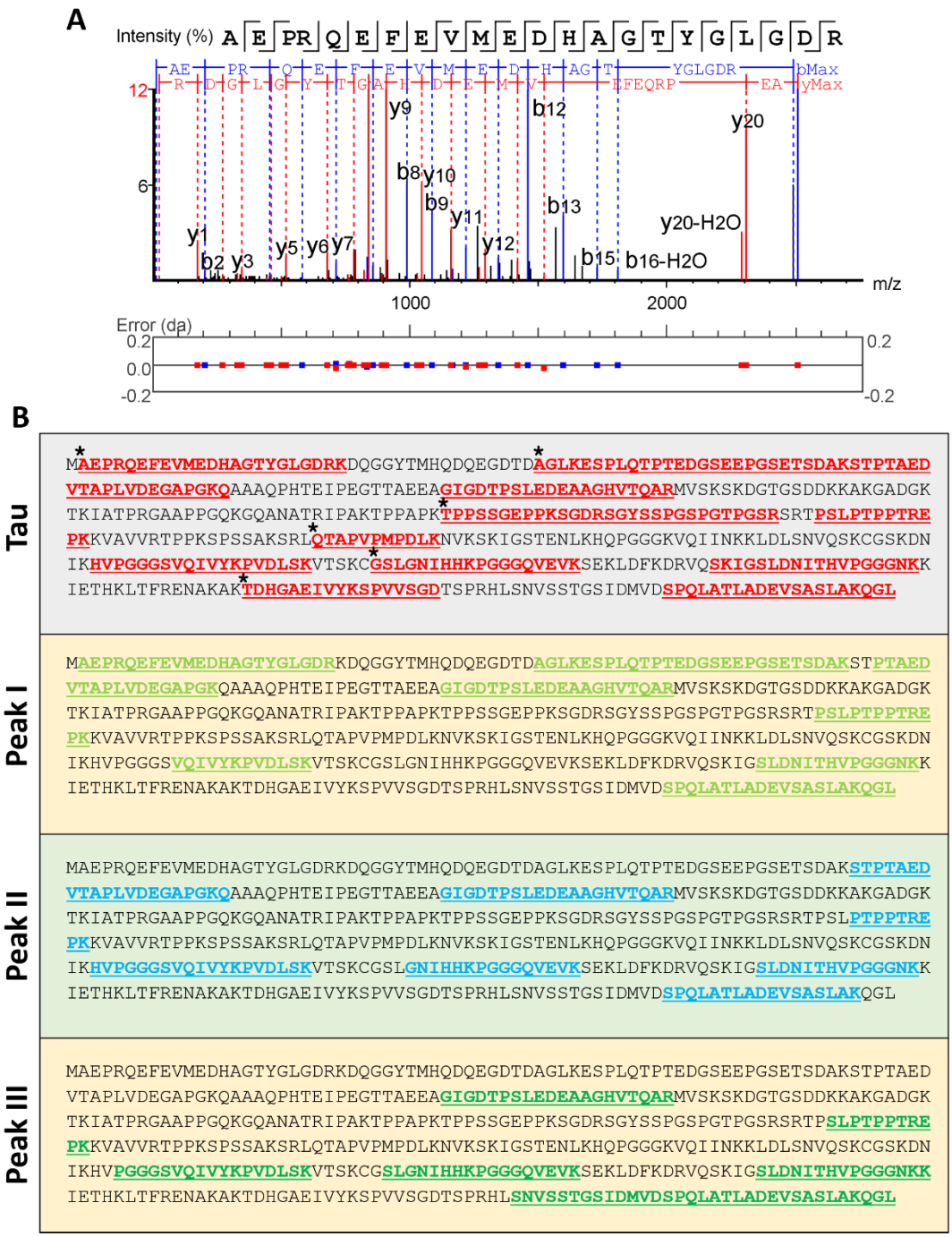

Figure 3. Mass spectrometry analysis of tau metabolites. A: Example of an MS spectrum corresponding to a tryptic peptide derived from 2N4R tau (AEPRQEFEVMEDHAGTYGGLGDR), b- and y-ions are labelled. **B:** 2N4R tau sequences and tryptic peptides, which could be identified in the corresponding samples, are highlighted. Asterisks label tryptic 2N4R tau peptides, which could not be identified in the three peak samples.

The tau degradation can explain that tryptic tau peptides are no longer detectable by 3CL^{pro} into different fragments, which may influence the composition and number of tryptic tau peptides in the four tested samples, as shown in Table 2.

Table 2. The number of tryptic tau peptides in control and the tested HPLC samples.

Sample	Number tryptic peptides	Peptides with the highest appearance
2N4R tau	111	AEPRQEFEVMEDHAGTYGGLGDR (8x)
I	66	SPQLATLADEVSASLAK (8x)
II	46	GDTPSLEDEAAGHVTQAR (6x)
II	63	SPQLATLADEVSASLAK (15x)

2N4R tau contains a sequence $_{241}$SRLQTAPV$_{248}$ (QTAPVPMPDLK tryptic peptide absent in peak I) which shows similarities to the preferred 3CL^{pro} cleavage pattern (Supplementary Fig. S7). A tau cleavage at this site could generate two fragments with sizes of 25 and 20 kDa, shown on the SDS page for peak I (Fig. 2C and 2E). Furthermore, at the N-terminus of tau, there are several potential cleavage sites for 3CL^{pro}, which can generate fragments with molecular weights between 45 and 27 kDa. Possible 3CL^{pro} cleavage sites relating to the tau protein sequence are shown in Supplementary Figure S7; this analysis is based on the amino acid preference in the SARS-CoV-2 3CL^{pro} substrate binding site (Information conceived from the Merops database) [48] and similar amino acid sequences in the tau sequence. Four sequences showed similarities with the 3C-like protease from coronavirus-2 and one with a 3C-like peptidase from strawberry mottle virus (Supplementary fig. S7).

The results described in this study indicated that 2N4R tau is proteolytically cleaved by 3CL^{pro,} and the cleavage is related to tau aggregation events. It has previously been described that tau proteolysis is associated with aggregation and that the tau protein has cleavage sites for different proteolytic enzymes [34] (Table 3).

Table 3. Examples of proteases with proteolytic activity against tau.

Protease	Cleavage site	Reference
Caspase-6	D13-H14	[49]
Caspase-3	D25-Q26; K44-E45	[50]
Calpain-1 and -2	R230-T231	[51,52]
Caspase-2	D314-L315	[53]
Calpain-1	K44-E45, R242-L243	[54,55]
ADAM10	A152-T153	[56]
Thrombin	R155-G156; R209-S210	[57]
Chymotrypsin	Y197-S198	[58]
Asparagine endopeptidase	N255-V256; N368-K369	[59]
Caspase-1, -3, -6, -7 and -8	D421-S422	[60]

Surface-based fluorescence intensity distribution analysis

Surface-based fluorescence intensity distribution analysis (sFIDA) was performed to quantify the tau oligomers and aggregates after treatment with 3CL^{pro}. The technique employs a similar biochemical setup as ELISA-like techniques. However, sFIDA uses the same epitope to capture and detect antibodies and features single-particle sensitivity through a microscopy-based readout (Herrmann et al., 2017). Recently, sFIDA was applied to quantify tau aggregates in cerebrospinal fluid (CSF) and

demonstrated its applicability in clinical settings [37]. Initial sFIDA experiments include analysis of tau monomers, tau aggregates and tau SiNaPs (Fig. 4A-C). To quantify tau aggregates formed by 3CL^{pro} proteolysis, two approaches were tested: tau plus active 3CL^{pro} and tau plus inactivated 3CL^{pro} (with the addition of disulfiram). As shown in Fig. 4D, Tau samples containing active 3CL^{pro} yielded higher aggregate-specific readouts than Tau samples in presence of inactivated protease. Compared to the Tau aggregate control, however, only a small fraction of the employed Tau substrate was converted into aggregates.

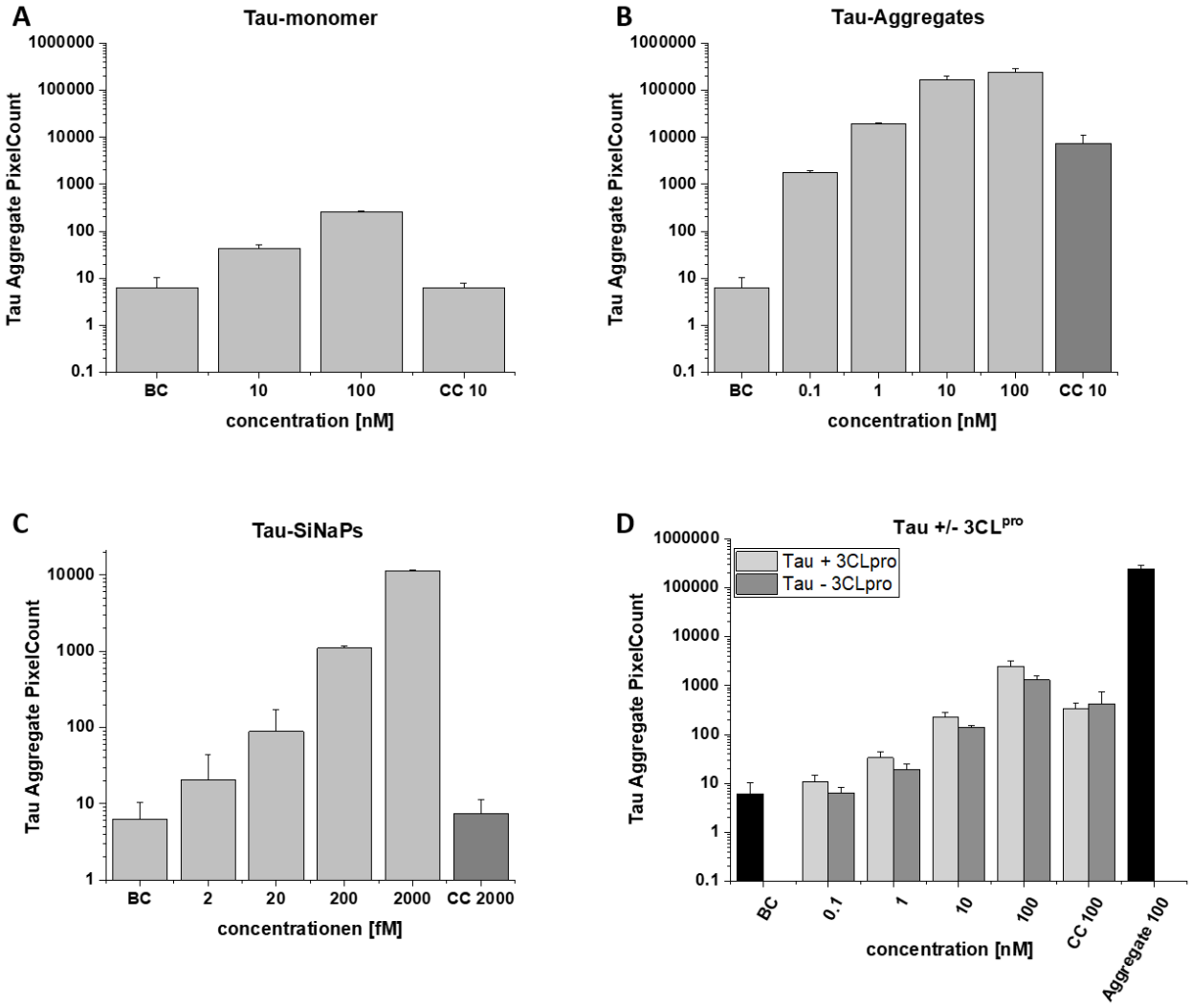

Figure 4. sFIDA experiments. Samples, buffer control (BC) and capture control (CC) were tested. Pixel counts per concentration are shown for **A:** Tau monomer control, **B:** Tau aggregate control, **C:** Tau SiNaPs and **D:** Influence of active 3CL^{pro} on tau aggregation.

It is well known that the structural diversity of tau aggregates can make their detection technically challenging [61].

For the sFIDA experiments anti-tau12 and anti-tau13 (Biolegend) were used, and both antibodies interact with the N-terminal region of tau (Tau 6-18 and 15-25) [62]. According to the mass spec results described before, tau epitope regions for anti-tau12 and anti-tau13 are cleaved and therefore cannot

react with the respective antibodies in the sFIDA assays. Additionally, remaining epitopes might be masked by aggregate core formation and can therefore not any more detected by the employed antibody system.

Conclusion and future work

The proportion of older adults in the population is increasing in almost all countries. Worldwide, around 55 million people have dementia, which is expected to increase to 78 million in 2030 and 139 million in 2050 [63]. Different dementias show a conformationally altered concentration of tau. Tau detaches from microtubules and aggregates into oligomers and neurofibrillary tangles, which can be secreted from neurons, and spread through the brain during disease progression.

The COVID-19 pandemic has increasingly moved virus infections into the scientific spotlight and has shown that this infection can damage the brain in many ways. The molecular underpinnings of neurodegenerative processes need to be investigated to develop appropriate therapies. Proteolysis of tau protein may be a crucial factor in forming toxic aggregates. Our results demonstrated that the SARS-CoV-2 $3CL^{pro}$ could cleave 2N4R tau into fragments and thus induce protein aggregation *in vitro*. However, further experiments need to be performed to get a closer assessment of the tau cleavage by SARS-CoV-2 $3CL^{pro}$:

- Adjustment and optimisation of sFIDA assay (e.g. antibodies).
- Cleavage and accessibility of tau binding regions for specific antibodies.
- Cell toxicity of tau peptides and related aggregates.
- *In vivo* experiments will confirm the role of the $3CL^{pro}$ on tau cleavage and aggregation.

Conflict of interest

The authors declare that no conflict of interest exists.

Acknowledgements

We want to thank the support of the Institute of Biological Information Processing (IBI-7) Forschungszentrum Jülich, Germany.

Author contributions

Conceptualisation, R.J.E; methodology, R.J.E., M.A.C., I.G., K.K., A.S., V.K.S. and L.B.; validation, R.J.E., I.G., A.S. and V.K.S.; formal analysis, R.J.E., I.G., A.S. and V.K.S.; investigation, R.J.E. and M.A.C.; re-sources, K.S., O.B. and D.W.; writing—original draft preparation, R.J.E.; writing—review and editing, R.J.E., M.A.C., I.G., K.K., A.S., K.S., V.K.S., L.B.; O.B., and D.W.; supervision, R.J.E.; all authors have read and agreed to the published version of the manuscript.

Funding

D.W. is supported by Deutsche Forschungsgemeinschaft (DFG, German Research Foundation), Project-ID 267205415, SFB 1208. sFIDA was supported by the programs “Biomarkers Across Neurodegenerative Diseases I + II” of The Alzheimer’s Association, Alzheimer’s Research UK and the Weston Brain Institute (11084 and BAND-19-614337). We are also grateful for support from The Michael J. Fox Foundation for Parkinson’s Research (14977, 009889), from the ALS Association and from the Packard Center (19-SI-476). We received further funding from the Deutsche Forschungsgemeinschaft (INST 208/616-1 FUGG, INST 208/794-1 FUGG) and the Helmholtz Association (HVF0079).

Data Availability Statement

All data and material will become available upon publication; additional data supporting this study's findings are available from the corresponding author R.J.E.

References

[1] Kim D, Lee JY, Yang JS, Kim JW, Kim VN, Chang H (2020) The Architecture of SARS-CoV-2 Transcriptome. Cell 181:914–921.e10 https://doi.org/10.1016/j.cell.2020.04.011

[2] Dai W, Zhang B, Jiang XM, Su H, Li J, Zhao Y, Xie X, Jin Z, Peng J, Liu F, Li C (2020) Structure-based design of antiviral drug candidates targeting the SARS-CoV-2 main protease. Science 368:1331-1335 https://doi.org/10.1126/science.abb4489

[3] Shin D, Mukherjee R, Grewe D, Bojkova D, Baek K, Bhattacharya A, Schulz L, Widera M, Mehdipour AR, Tascher G, et al. (2020) Papain-like protease regulates SARS-CoV-2 viral spread and innate immunity. Nature 587:657–662 https://doi.org/10.1038/s41586-020-2601-5

[4] Jagdeo JM, Dufour A, Klein T, Solis N, Kleifeld O, Kizhakkedathu J, Luo H, Overall CM, Jan E (2018) N-Terminomics TAILS IdentifiesHost Cell Substrates of Poliovirus and Coxsackievirus B3 3C Proteinases That Modulate Virus Infection. J Virol 92:e02211–e02217 https://doi.org/10.1128/JVI.02211-17

[5] Stukalov A, Girault V, Grass V, Karayel O, Bergant V, Urban C, Haas DA, Huang Y, Oubraham L, Wang A, et al. (2021) Multilevel proteomics reveals host perturbations by SARS-CoV-2 and SARS-CoV. Nature 594:246–252 https://doi.org/10.1038/s41586-021-03493-4

[6] Bouhaddou M, Memon D, Meyer B, White KM, Rezelj VV, Correa Marrero M, Polacco BJ, Melnyk JE, Ulferts S, Kaake RM et al. (2020) The Global Phosphorylation Landscape of SARS-CoV-2 Infection. Cell 182:685–712.e19 https://doi.org/10.1016/j.cell.2020.06.034

[7] Gordon DE, Jang GM, Bouhaddou M, Xu J, Obernier K, White KM, O'Meara MJ, Rezelj VV, Guo JZ, Swaney DL, Tummino TA, et al. (2020) A SARS-CoV-2 protein interaction map reveals targets for drug repurposing. Nature 583:459–468 https://doi.org/10.1038/s41586-020-2286-9

[8] Lopez-Otın C, Overall CM (2002) Protease degradomics: a new challenge for proteomics. Nat Rev Mol Cell Biol 3:509–519 https://doi.org/10.1038/nrm858

[9] Pablos I, Machado Y, de Jesus HCR, Mohamud Y, Kappelhoff R, Lindskog C, Vlok M, Bell PA, Butler GS, Grin PM, Cao QT (2021) Mechanistic insights into COVID-19 by global analysis of the SARS-CoV-2 3CLpro substrate degradome. Cell Rep 37:109892 https://doi.org/10.1016/j.celrep.2021.109892

[10] Wu F, Zhao S, Yu B, Chen YM, Wang W, Song ZG, Hu Y, Tao ZW, Tian JH, Pei YY, Yuan ML, Zhang YL, Dai FH, et al. (2020) A new coronavirus associated with human respiratory disease in China. Nature 579:265–269 https://doi.org/10.1038/s41586-020-2202-3

[11] WHO. 2023. World Health Organization, Coronavirus disease 2019 (COVID-19) Dashboard, 03.01.2023.

[12] Yin Y, Wunderink RG (2018) MERS, SARS and other coronaviruses as causes of pneumonia. Respirology. 23:130–137 https://doi.org/10.1111/resp.13196

[13] Giannis D, Ziogas I, Gianni P (2020) Coagulation disorders in coronavirus infected patients: COVID-19, SARS-CoV-1, MERS-CoV and lessons from the past. J Clin Virol 127:104362 https://doi.org/10.1016/j.jcv.2020.104362

[14] Li H, Liu L, Zhang D, Xu J, Dai H, Tang N, Su X, Cao B (2020) SARS-CoV-2 and viral sepsis: Observations and hypotheses. Lancet 395:1517–1520 https://doi.org/10.1016/S0140-6736(20)30920-X

[15] Lin L, Jiang X, Zhang Z, Huang S, Zhang Z, Fang Z, Gu Z, Gao L, Shi H, Mai L, Liu Y, Lin X, Lai R, Yan Z, Li X, Shan H (2020) Gastrointestinal symptoms of 95 cases with SARS-CoV-2 infection. Gut 69:997–1001 https://doi.org/10.1136/gutjnl-2020-321013

[16] Baig AM (2020) Neurological manifestations in COVID-19 caused by SARS-CoV-2. CNS Neurosci Ther 26:499–501 https://doi.org/10.1111/cns.13372

[17] Mahase E (2020) Covid-19: What do we know about "long covid"? Brit Med J 14:370 https://doi.org/10.1136/bmj.m2815

[18] Halpin S, O'Connor R, Sivan M (2021) Long COVID and chronic COVID syndromes. J Med Virol 93:1242-1243 https://doi.org/10.1002/jmv.26587

[19] Shelton JF, Shastri AJ, Fletez-Brant K, Aslibekyan S, Auton A (2022) The UGT2A1/UGT2A2 locus is associated with COVID-19-related loss of smell or taste. Nat Genet 54:121-124 https://doi.org/10.1038/s41588-021-00986-w

[20] Chan JL, Murphy KA, Sarna JR (2021) Myoclonus and cerebellar ataxia associated with COVID-19: a case report and systematic review. J Neurol 268:3517-3548 https://doi.org/10.1007/s00415-021-10458-0

[21] Cartella S, Terranova C, Arena I, Quartarone A, Girlanda P (2021) Impact of Covid-19 on essential tremor and dystonic tremor: Experience of an Italian centre. J Neurol Sci 429:119437 https://doi.org/10.1016/j.jns.2021.119437

[22] Kacprzak A, Malczewski D, Domitrz I (2021) Headache Attributed to SARS-CoV-2 Infection or COVID-19 Related Headache—Not Migraine-like Problem-Original Research. Brain Sci 11:1406 https://doi.org/10.3390/brainsci11111406

[23] Baig AM, Khaleeq A, Ali U, Syeda H (2020) Evidence of the COVID-19 Virus Targeting the CNS: tissue distribution, host-virus interaction, and proposed neurotropic mechanisms. ACS Chem Neurosci 11:995-998 https://doi.org/10.1021/acschemneuro.0c00122

[24] Uginet M, Breville G, Assal F, Lövblad KO, Vargas MI, Pugin J, Serratrice J, Herrmann FR, Lalive PH, Allali G (2021) COVID-19 encephalopathy: Clinical and neurobiological features. J Med Virol 93:4374-4381 https://doi.org/10.1002/jmv.26973

[25] Mahapure KS, Prabhune AS, Chouvhan AV (2021) COVID-19-associated acute disseminated encephalomyelitis: A systematic review. Asian J Neurosurg 16:457 https://doi.org/10.4103/ajns.AJNS_406_20

[26] Nannoni S, de Groot R, Bell S, Markus HS (2021) Stroke in COVID-19: a systematic review and meta-analysis. Int J Stroke 16:137-149 https://doi.org/10.1177/1747493020972922

[27] Khan F, Sharma P, Pandey S, Sharma D, Kumar N, Shukla S, Dandu H, Jain A, Garg RK, Malhotra HS (2021) COVID-19-associated Guillain-Barre syndrome: Postinfectious alone or neuroinvasive too? J Med Virol 93:6045-6049 https://doi.org/10.1002/jmv.27159

[28] Douaud G, Lee S, Alfaro-Almagro F, Arthofer C, Wang C, McCarthy P, Lange F, Andersson JL, Griffanti L, Duff E, et al. (2022) SARS-CoV-2 is associated with changes in brain structure in UK Biobank. Nature 604:697-707 https://doi.org/10.1038/s41586-022-04569-5

[29] Ross CA, Poirier MA (2004) Protein aggregation and neurodegenerative disease. Nat Med 10(Suppl):S10–S17 https://doi.org/10.1038/nm1066

[30] Sun B, Tang N, Peluso MJ, Iyer NS, Torres L, Donatelli JL, Munter SE, Nixon CC, Rutishauser RL, Rodriguez-Barraquer I, et al. (2021) Characterisation and biomarker analyses of post-covid-19 complications and neurological manifestations. Cells 10:386 https://doi.org/10.3390/cells10020386

[31] Idrees D, Kumar V (2021) SARS-CoV-2 spike protein interactions with amyloidogenic proteins: Potential clues to neurodegeneration. Biochem Biophys Res Commun 554:94–98 https://doi.org/10.1016/j.bbrc.2021.03.100

[32] Tavassoly O, Safavi F, Tavassoly I (2020) Seeding brain protein aggregation by SARS-CoV-2 as a possible long-term complication of COVID-19 infection. ACS Chem Neurosci 11:3704–3706 https://doi.org/10.1021/acschemneuro.0c00676

[33] Ramani A, Müller L, Ostermann PN, Gabriel E, Abida-Islam P, Müller-Schiffmann A, Mariappan A, Goureau O, Gruell H, et al. (2020) SARS-CoV-2 targets neurons of 3D human brain organoids. EMBO J 39:p.e106230 https://doi.org/10.15252/embj.2020106230

[34] Quinn JP, Corbett NJ, Kellett KA, Hooper NM (2018) Tau proteolysis in the pathogenesis of tauopathies: neurotoxic fragments and novel biomarkers. J Alzheimer's Dis 63:13-33 https://doi.org/10.3233/JAD-170959

[35] Hoyer W, Antony T, Cherny D, Heim G, Jovin TM, Subramaniam V (2002) Dependence of α-synuclein aggregate morphology on solution conditions. J Mol Biol 322:383-393 https://doi.org/10.1016/S0022-2836(02)00775-1

[36] Margittai M, Langen R (2004) Template-assisted filament growth by parallel stacking of tau. Proc Natl Acad Sci USA 101:10278-10283 https://doi.org/10.1073/pnas.0401911101

[37] Blömeke L, Pils M, Kraemer-Schulien V, Dybala A, Schaffrath A, Kulawik A, Rehn F, Cousin A, Nischwitz V, Willbold J, Zack R (2022) Quantitative detection of α-Synuclein and Tau oligomers and other aggregates by digital single particle counting. NPJ Parkinsons Dis 8:1-13 https://doi.org/10.1038/s41531-022-00330-x

[38] Eberle RJ, Olivier DS, Amaral MS, Gering I, Willbold D, Arni RK, Coronado MA (2021) The Repurposed Drugs Suramin and Quinacrine Cooperatively Inhibit SARS-CoV-2 $3CL^{pro}$ *In Vitro*. Viruses 13:873 https://doi.org/10.3390/v13050873

[39] Kravchenko K, Kulawik A, Hülsemann M, Kühbach K, Zafiu C, Herrmann Y, Linnartz C, Peters L, Bujnicki T, et al. (2017) Analysis of anticoagulants for blood-based quantitation of amyloid β oligomers in the sFIDA assay. Biol Chem 398:465-75 https://doi.org/10.1515/hsz-2016-0153

[40] Herrmann Y, Bujnicki T, Zafiu C, Kulawik A, Kühbach K, Peters L, Fabig J, Willbold J, Bannach O, Willbold D (2017) Nanoparticle standards for immuno-based quantitation of α-synuclein oligomers in diagnostics of Parkinson's disease and other synucleinopathies. Clin Chim 466:152-159 https://doi.org/10.1016/j.cca.2017.01.010

[41] Hülsemann M, Zafiu C, Kühbach K, Lühmann N, Herrmann Y, Peters L, Linnartz C, Willbold J, Kravchenko K, et al. (2016) Biofunctionalised silica nanoparticles: standards in amyloid-β oligomer-based diagnosis of Alzheimer's disease. J Alzheimer's Dis 54:79-88 https://doi.org/10.3233/JAD-160253

[42] Yao TM, Tomoo K, Ishida T, Hasegawa H, Sasaki M, Taniguchi T (2003) Aggregation analysis of the microtubule binding domain in tau protein by spectroscopic methods. J Biochem (Tokyo) 134:91–99 https://doi.org/10.1093/jb/mvg116

[43] von Bergen M, Barghorn S, Biernat J, Mandelkow EM, Mandelkow E (2005) Tau aggregation is driven by a transition from random coil to beta sheet structure. Biochim Biophys Acta BBA Mol Basis Dis 1739:158–166 https://doi.org/10.1016/j.bbadis.2004.09.010

[44] Karikari TK, Turner A, Stass R, Lee LCY, Wilson B, Nagel DA, Hill EJ, Moffat KG (2017) Expression and purification of tau protein and its frontotemporal dementia variants using a cleavable histidine tag. Protein Expr Purif 130:44-54 https://doi.org/10.1016/j.pep.2016.09.009

[45] Barghorn S, Zheng-Fischhöfer Q, Ackmann M, Biernat J, von Bergen M, Mandelkow EM, Mandelkow E (2000) Structure, microtubule interactions, and paired helical filament aggregation by tau mutants of frontotemporal dementias. Biochemistry 39:11714–11721 https://doi.org/10.1021/bi000850r

[46] Luo J, He R, Li W (2000) The fluorescent characterisation of the polymerised microtubule-associated protein Tau. Int J Biol Macromol 27:263-268 https://doi.org/10.1016/S0141-8130(00)00126-4

[47] Lobo-Galo N, Terrazas-López M, Martínez-Martínez A, Díaz-Sánchez ÁG (2021) FDA-approved thiol-reacting drugs that potentially bind into the SARS-CoV-2 main protease, essential for viral replication. J Biomol Struct Dyn 39:3419-3427 https://doi.org/10.1080/07391102.2020.1764393

[48] Rawlings ND, Barrett AJ, Thomas PD, Huang X, Bateman A, Finn RD (2018) The MEROPS database of proteolytic enzymes, their substrates and inhibitors in 2017 and a comparison with peptidases in the PANTHER database. Nucleic Acids Res 46(D1):D624-D632 https://doi.org/10.1093/nar/gkt953

[49] Horowitz PM, Patterson KR, Guillozet-Bongaarts AL, Reynolds MR, Carroll CA, Weintraub ST, Bennett DA, et al. (2004) Early N-terminal changes and caspase-6 cleavage of tau in Alzheimer's disease. J Neurosci 24:7895–7902 https://doi.org/10.1523/JNEUROSCI.1988-04.2004

[50] Amadoro G, Ciotti MT, Costanzi M, Cestari V, Calissano P, Canu N (2006) NMDA receptor mediates tau-induced neurotoxicity by calpain and ERK/MAPK activation. Proc Natl Acad Sci USA 103:2892–2897 https://doi.org/10.1073/pnas.0511065103

[51] Park SY, Ferreira A (2005) The generation of a 17 kDa neurotoxic fragment: An alternative mechanism by which tau mediates beta-amyloid-induced neurodegeneration. J Neurosci 25:5365–5375 https://doi.org/10.1523/JNEUROSCI.1125-05.2005

[52] Garg S, Timm T, Mandelkow EM, Mandelkow E, Wang Y (2010) Cleavage of Tau by calpain in Alzheimer's disease: The quest for the toxic 17 kD fragment. Neurobiol Aging 32:1–14 https://doi.org/10.1016/j.neurobiolaging.2010.09.008

[53] Zhao X, Kotilinek LA, Smith B, Hlynialuk C, Zahs K, Ramsden M, Cleary J, Ashe KH (2016) Caspase-2 cleavage of tau reversibly impairs memory. Nat Med 22:1268–1276 https://doi.org/10.1038/nm.4199

[54] Yang LS, Ksiezak-Reding H (1995) Calpain-induced proteolysis of normal human tau and tau associated with paired helical filaments. Eur J Biochem 233:9–17 https://doi.org/10.1111/j.1432-1033.1995.009_1.x

[55] Matsumoto SE, Motoi Y, Ishiguro K, Tabira T, Kametani F, Hasegawa M, Hattori N (2015) The twenty-four KDa C-terminal tau fragment increases with aging in tauopathy mice: Implications of prion-like properties. Hum Mol Genet 24:6403–6416 https://doi.org/10.1093/hmg/ddv351

[56] Henriksen K, Wang Y, Sorensen MG, Barascuk N, Suhy J, Pedersen JT, Duffin KL, Dean RA, Pajak M, et al. (2013) An enzyme-generated fragment of tau measured in serum shows an inverse correlation to cognitive function. PLoS One 8:e64990 https://doi.org/10.1371/journal.pone.0064990

[57] Arai T, Guo JP, McGeer PL (2005) Proteolysis of non-phosphorylated and phosphorylated tau by thrombin. J Biol Chem 280:5145–5153 https://doi.org/10.1074/jbc.M409234200

[58] Steiner B, Mandelkow EM, Biernat J, Gustke N, Meyer HE, Schmidt B, Mieskes G, Soling HD, Drechsel D, et al. (1990) Phosphorylation of microtubule-associated protein tau: Identification of the site for Ca2(+)-calmodulin dependent kinase and relationship with tau phosphorylation in Alzheimer tangles. EMBO J 9:3539–3544 https://doi.org/10.1002/j.1460-2075.1990.tb07563.x

[59] Zhang Z, Song M, Liu X, Kang SS, Kwon IS, Duong DM, Seyfried NT, Hu WT, Liu Z, Wang JZ, Cheng L, et al. (2014) Cleavage of tau by asparagine endopeptidase mediates the neurofibrillary pathology in Alzheimer's disease. Nat Med 20:1254–1262 https://doi.org/10.1038/nm.3700

[60] Gamblin TC, Chen F, Zambrano A, Abraha A, Lagalwar S, Guillozet AL, Lu M, Fu Y, Garcia-Sierra F, et al. (2003) Caspase cleavage of tau: Linking amyloid and neurofibrillary tangles in Alzheimer's disease. Proc Natl Acad Sci USA 100:10032–10037 https://doi.org/10.1073/pnas.1630428100

[61] Alam P, Bousset L, Melki R, Otzen DE (2019) Alpha-synuclein oligomers and fibrils: A spectrum of species, a spectrum of toxicities. J Neurochem 150:522–534 https://doi.org/10.1111/jnc.14808

[62] Sengupta U, Portelius E, Hansson O, Farmer K, Castillo-Carranza D, Woltjer R, Zetterberg H, Galasko D, et al. (2017) Tau oligomers in cerebrospinal fluid in Alzheimer's disease. Ann Clin Transl Neurol 4:226-235 https://doi.org/10.1002/acn3.382

[63] Nichols E, Steinmetz JD, Vollset SE, Fukutaki K, Chalek J, Abd-Allah F, Abdoli A, Abualhasan A, Abu-Gharbieh E, et al. (2022) Estimation of the global prevalence of dementia in 2019 and forecasted prevalence in 2050: an analysis for the Global Burden of Disease Study 2019. Lancet Glob Health 7:e105-e125 https://doi.org/10.1016/S2468-2667(21)00249-8